



## **Residual capacity of RC beams subjected to impact loading: Influence of reinforcement ductility**

Downloaded from: <https://research.chalmers.se>, 2024-09-27 08:20 UTC

Citation for the original published paper (version of record):

Johansson, M., Leppänen, J., Andersson, M. et al (2024). Residual capacity of RC beams subjected to impact loading: Influence of reinforcement ductility. *International Journal of Protective Structures*, In Press. <http://dx.doi.org/10.1177/20414196241277221>

N.B. When citing this work, cite the original published paper.

# Residual capacity of RC beams subjected to impact loading: Influence of reinforcement ductility

Morgan Johansson<sup>1,2</sup> , Joosef Leppänen<sup>2</sup>,  
Malin Andersson<sup>3</sup> and Emma Pettersson<sup>3</sup>

International Journal of Protective  
Structures  
2024, Vol. 0(0) 1–18  
© The Author(s) 2024



Article reuse guidelines:  
[sagepub.com/journals-permissions](https://sagepub.com/journals-permissions)  
DOI: [10.1177/20414196241277221](https://doi.org/10.1177/20414196241277221)  
[journals.sagepub.com/home/prs](https://journals.sagepub.com/home/prs)



## Abstract

Reinforced concrete (RC) is commonly used for protective structures subjected to impulse loading and in the design of such structures, knowledge gained from static load conditions is often used. However, the response of an impulse loaded structural member may be very different compared to a statically loaded one, and hence it is not for sure that the observations made at static loading are also valid when subjected to impulse loading. The aim of this study is to address this uncertainty and compare the residual capacity, in terms of strength and internal work, in RC beams subjected to a combination of impulse and static loads or static load only. The impulse load was generated using a drop weight impact in which tests of 12 beams were carried out, and the residual capacity was subsequently tested statically. In addition, six beams were subjected to static loading only as references. The beams were simply supported with a span length of 1.3 m, cross section of 0.1 × 0.1 m and 2 + 2  $\phi$ 6 reinforcement bars of various ductility. Two sets of bars were used: regular bars and prestretched bars; the latter being cold-worked regular bars with increased yield strength but decreased ductility. The drop weight (10 kg or 20 kg) was dropped from a height of 5.0 m and a high-speed camera used to record the beams' response. From the images obtained, Digital Image Correlation technique was used to measure deformations and crack propagation. For pure static loading and mild impact loading (10 kg) combined with static loading, beams with regular bars obtained higher internal work than beams with prestretched bars. However, for severe impact loading (20 kg) combined with static loading, the difference in internal work was negligible. Regardless of bar type, the internal work increased with increased severity of the impact loading.

## Keywords

Reinforced concrete, impact loading, reinforcement ductility, residual capacity, internal work

<sup>1</sup>Norconsult AB, Gothenburg, Sweden

<sup>2</sup>Architecture and Civil Engineering, Chalmers University of Technology, Gothenburg, Sweden

<sup>3</sup>ELU Konsult AB, Gothenburg, Sweden

## Corresponding author:

Morgan Johansson, Norconsult AB, Theres Svenssons gata 11, Gothenburg SE-417 55, Sweden.

Email: [morgan.johansson@norconsult.com](mailto:morgan.johansson@norconsult.com)

## Introduction

Reinforced concrete (RC) is commonly used for protective structures subjected to impulse loading. This is due to its high mass and potential high energy absorption, in which the latter is thanks to the structure's ability to withstand large plastic deformations with remaining load capacity. In the design of such structures, knowledge gained from static loading is often used. However, the response of an impulse loaded structure may be very different compared to a statically loaded one (Magnusson et al., 2014), and hence it is not for sure that the observations made at static loading are also valid for impulse loading.

The reasons for difference in response at impulse- and static loading are due to a combination of inertia, strain rate and wave propagation effects that may appear in the former. Inertia resists the change in motion and thus provide extra resistance to the structure while strain rate effects make the material stronger, stiffer and less ductile (Bischoff and Perry, 1991; Malvar and Ross, 1998). Further, wave propagation effects, that is, the transformation of information within the loaded structure, may cause the structure to respond differently both locally and globally (Cotsovos et al., 2008; Isaac et al., 2017; Pham and Hao, 2017). Even so, it is common to base the design of impulse loaded structures on knowledge gained from static loading, for example, the bending moment capacity or plastic deformation capacity (DOD, 2008; Fortifikationsverket, 2011; Johansson and Rempling, 2016).

Generally, impulse loading is caused by the blast wave from an explosion, or an impact caused by an object striking into the structure at a given velocity. The loading characteristics of such events may differ considerably, but the structural response of the affected structure is in many ways still similar. Hence, when studying the structural response of an impulse loaded structure it is often possible to use a more simplified test set-up, consisting of a drop weight impact, rather than that necessary to simulate the blast load generated by an explosion.

The design of impulse loaded structures often relies upon large plastic deformation capacities, that is, the internal work of the structure is provided by large deformations rather than large load capacity. Hence, it is essential that the internal work assumed in the design is also relevant for the actual load case. However, since the structural response of an impulse loaded structure may be different compared to when statically loaded, the plastic deformation capacity and failure modes of the structure may also be different when subjected to impulse loading. Consequently, it is of interest to make sure that the observations obtained from static loading, regarding internal work, are also valid for dynamic loading. The ductility properties of the steel reinforcement, that is, ratio  $f_t/f_y$  between the ultimate strength and the yield strength, and strain  $\epsilon_u$  at ultimate strength, are important parameters to obtain large plastic deformation capacity (CEB, 1998), and thus internal work, in concrete structures.

The aim of this study is to examine how the internal work of reinforced concrete beams is affected by impulse loading and mechanical properties of reinforcement. To simplify, drop weight impact tests were used to simulate the impulse loading. Similar conceptual studies have been carried out by several researchers, for example, Saatchi et al. (2009), Fujikake et al. (2009), Ulzurun and Zanuy (2017), Peterson and Ansell (2022), to study the dynamic structural response of concrete structures. Here, though, the impact loading was also combined with static loading applied after the impact tests, investigating the residual capacity of the damaged beams. Similar studies have been done by for example, Fujikake et al. (2006) and Adhikary et al. (2015), but there the focus has not been on the residual static capacity and the number of static follow-up tests have been limited.

## Drop weight impact and static tests

### Test series and test set-up

The test series consisted of 18 beams with denotations in accordance with Table 1. The beams in Series I10 (Series I20) were first subjected to an impact test with a drop weight impact with a mass of 10 kg (20 kg), dropped from a height  $h = 5.0$  m (impact velocity  $v_0 \approx 9.9$  m/s) and thereafter, the beams were subjected to static load until failure. The results were compared with reference beams in Series S, which were subjected to static load only until failure. Series S and I10 were tested in three-point bending while Series I20 was tested in four-point bending using deformation-controlled loading. The reason for the different load conditions was that the latter beams, after impact loading, had a high level of concrete damage in the mid beam region, resulting in three-point bending being unsuitable for these beams.

Drop weight impact tests were conducted on 12 beams and static tests on 12 + 6 beams with test set-ups according to Figure 1. The beam length was 1 400 mm with a span length of 1 300 mm, and a cross-sectional area of 100 x 100 mm. All beams were reinforced with 2 + 2 longitudinal ribbed bars of steel class K500C-T with a nominal diameter of 6 mm, located with a distance of 20 mm from the centre of the bars to the concrete surface. The beams in the impact tests were supported on fixed half-cylindrical supports with a diameter of 70 mm. The aim in these tests was to use boundary conditions that were as well defined as possible, and hence no restraint for upward movement was used. The drop weight consisted of a non-solid steel cylinder with mass 10 or 20 kg (length: 260 mm or 510 mm, diameter 80 mm, radius at contact surface 200 mm). For further details of the experiments, see Andersson and Pettersson (2019) and Leppänen (2024).

For the concrete, the compressive strength and fracture energy were tested using cubes and wedge splitting tests, respectively. The resulting average values for (recalculated) cylinder strength was  $f_c = 41$  MPa and fracture energy was  $G_F = 113$  N/m at an age of 27 days (day of impact testing) and 36 days, respectively.

For the steel reinforcement, coiled bars of class B500C-T were used. To study the influence of the reinforcement ductility, two different types of slacked reinforcement were used: one consisting of regular bars and one of what is here denoted as prestretched bars. The latter was manufactured by stretching 6.0 m long regular bars until a plastic strain  $\epsilon_{pl} \approx 3.0$  % was obtained. Thereby, a cold worked version of the regular bars with increased proof strength  $f_{0.2}$  but decreased ductility was created. After stretching, the prestretched bars were unloaded and cut in lengths of about 1.38 m

**Table 1.** Test Series.

Series	Specimen	Reinforcement type <sup>b</sup>	Type of test	Drop weight mass (kg)
S	B-01, B-02, B-03	Regular	Static (3-point bending)	-
	B-04, B-05, B-06	Prestretched		
I10	B-07, B-08, B-09	Regular	Impact + static (3-point bending)	10
	B-10, B-11, B-12	Prestretched		
I20	B-13, B-14, B-15 <sup>a</sup>	Regular	Impact + static (4-point bending)	20
	B-16, B-17, B-18	Prestretched		

<sup>a</sup>During impact testing, specimen B-15 was subjected to an unintentional impact when the cord, lifting the drop weight in the test set-up, snapped. Hence, this specimen was subjected to extra impact loading of uncertain magnitude and is therefore not included in the results presented here.

<sup>b</sup>Both regular and prestretched bars consisted of slack reinforcement. The prestretched bars consisted of a cold worked version of the regular bars but was not prestressed.

before being cast (without any external stress applied) into the concrete beams. Six bars of each type were tested and in [Figure 2](#) the stress-strain curves of a representative bar of each type are compared; the average values of the mechanical properties from all bars tested are presented in [Table 2](#). Further details of the reinforcement bars and the material tests are given in [Andersson and Petterson \(2019\)](#) and [Leppänen \(2024\)](#).

### High-speed camera and DIC

The structural response of all beams was analysed using Digital Image Correlation (DIC). The basic idea behind DIC is to measure the deformation of a specimen during testing by analysing the deformation of a surface provided with a speckle pattern in a series of digital images acquired during loading. This is accomplished by tracking the position of discrete pixel subsets of the speckle pattern

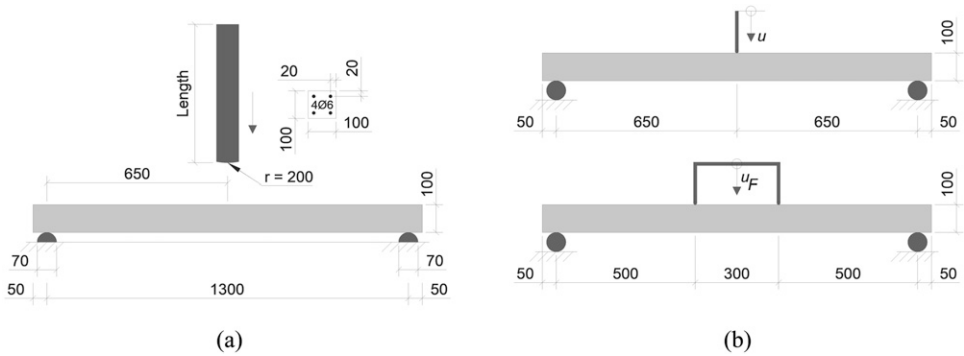


**Figure 1.** Test setup for (a) drop weight impact tests, and (b) deformation controlled static tests in three-point bending (Series S and Series I10) and four-point bending (Series I20).

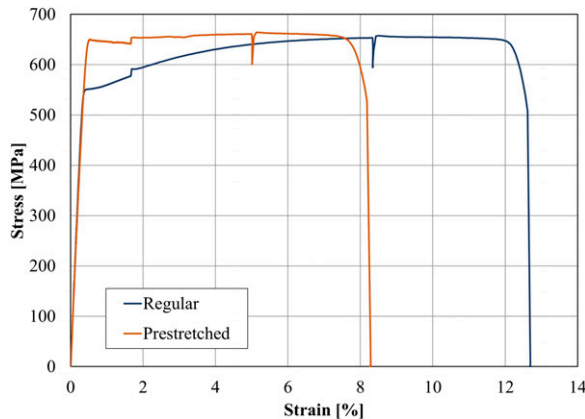


**Figure 2.** Stress-strain curve of representative reinforcement bars used in tests.

**Table 2.** Material Properties for Steel Reinforcement.

Reinforcement	$E_s$ (GPa)	$f_{0.2}$ (MPa)	$f_t$ (MPa)	$f_t/f_{0.2}$ [-]	$\varepsilon_u^a$ (%)
Regular	202	555	656	1.18	9.4
Prestretched	196	645	664	1.03	5.8

<sup>a</sup> $\varepsilon_u$  is defined as reinforcement strain when  $f_t$  is reached.

within the images. The deformations of the specimens are then calculated by correlating the positions and displacements of subsets in the undeformed reference image and the deformed images to produce a deformation vector field. A comprehensive description of this technique can be found in for example [Sutton et al. \(2009\)](#).

The impact tests of the beams were investigated using 2D-DIC technique with a Photron FASTCAM SA4 high-speed camera provided with a Tamron AF 28-75/2.8 lens, set to 50. The camera was placed at a perpendicular distance of approximately 1 980 mm from the surface of the tested beam and a camera resolution and image acquisition rate of  $1024 \times 400$  pixels and 5 000 frames per second (FPS), respectively, were used, corresponding to a time resolution of 0.2 ms. The camera configuration corresponded to a field of view of approximately 767 x 300 mm, that is, somewhat more than half the beam length. The images from the high-speed camera were analysed by DIC technique using the software [GOM Correlate \(n. d\)](#). The dimensions of each subset were 15 x 15 pixels, and the subset step was five pixels, which corresponds to a subset size and data point spacing of approximately 11.3 mm and 3.8 mm, respectively.

In the static loading tests, 3D-DIC measurements with a stereoscopic camera set-up were performed with the system ARAMIS 12M by [GOM Correlate \(n. d\)](#). The images were captured with a frequency of 0.5 FPS and the dimensions of each subset were 17 x 17 pixels and the subset step was 14 pixels. This corresponds to a subset size and a data point spacing of approximately 4.4 mm and 3.6 mm, respectively, at the surface of the beam.

## Results

### Response at impact loading

The initial response of a beam subjected to impact loading may be very different compared to that obtained in a beam subjected to static loading. In [Figure 3](#), the deformed shape at different stages of an impact loaded beam is schematically illustrated ([Leppänen et al., 2020](#)). This type of response was also obtained in the impact tests presented herein, see [Figure 4](#). Here, the relative deformation

$$u_{rel}(x, t) = \frac{u(x, t)}{u_{mid}(t)} \quad (1)$$

of beam B-07 is shown for the initial 2.0 ms after impact (a similar response was observed for all impact loaded beams). From this it is evident that the impact loaded beam initially does not obtain the typical triangular deformation shape expected for a statically loaded beam that exhibit a plastic hinge in the middle of the beam. Instead, the beam parts close to the supports are initially unaffected by the applied impact load, resulting in just the middle part of the beam

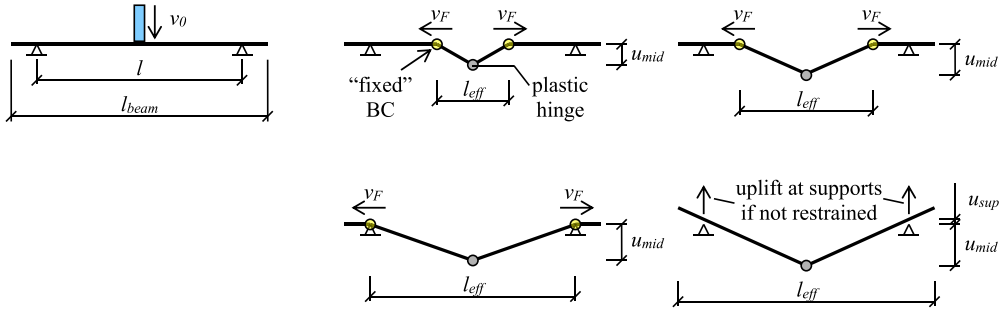


**Figure 3.** Schematic illustration of the initial dynamic response of an impact loaded beam not vertically restrained at the supports, based on Leppänen et al. (2020).

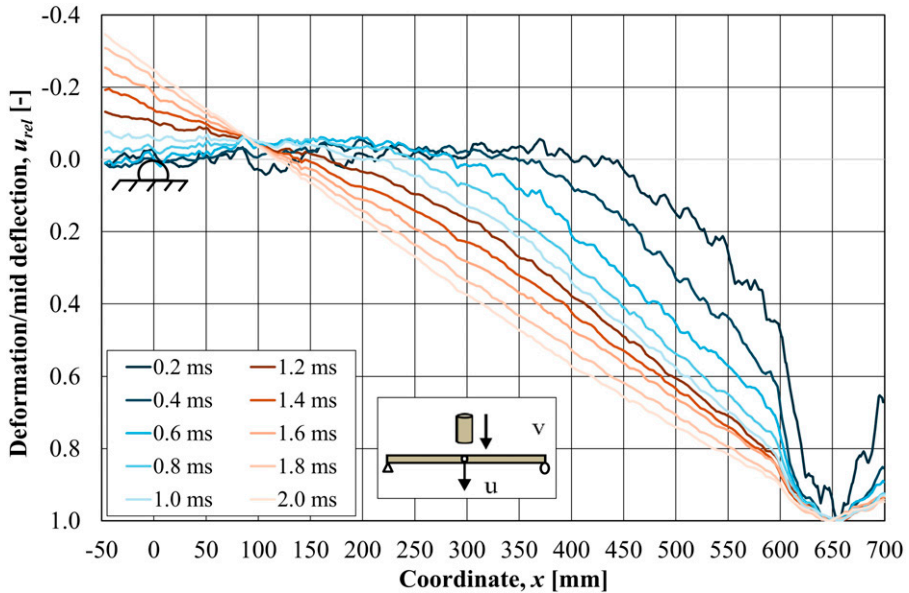


**Figure 4.** Ratio deformation/mid deflection of beam B-07 at different times after impact.

deforming. At time  $t = 0.2$  ms, this generates a local negative curvature next to the impact zone, approximately halfway to the support, and with time, this region with negative curvature moves towards the support. When the negative curvature reaches the support, uplift of the beam occurs since it is not vertically restrained. This phenomenon can be looked upon as the effect of time dependent boundary conditions, that is, the boundary conditions can approximately be regarded as fixed with the location of the fixity moving closer to the real support with time. Eventually, the beam becomes fully “aware” of its boundary conditions and the response then changes to something more like that of a statically loaded beam. For the beam in Figure 4 this change is completed after about 2 ms.

Using DIC, the resulting crack pattern in the beams can be indicated by showing the maximum principal strain field. In Figure 5 this is done, whereby the change in crack pattern during the initial response ( $t = 0.4\text{--}2.0$  ms) after impact are shown for all beams subjected to impact loading. The negative curvature obtained in the beam during the first millisecond, see Figure 4, results in tensile stresses which may cause cracking in the top of the beam. For times  $t = 0.4\text{--}0.8$  ms, such cracks are also seen in Figure 5. However, at time  $t = 2.0$  ms, the top cracks have closed again and cracks in the bottom of the beam have developed instead. In addition to the initial response, the resulting crack pattern at  $u_{max}$  is shown together with time of occurrence.

In Figure 4, it is shown that there is an initial uplift of the beam at the support. However, this uplift is only temporary, and the beam is soon pressed down in contact with the support again. In Figure 6, the uplift  $u_{sup}(t)$  at the support is presented together with the midpoint deflection  $u_{mid}(t)$  for beams B-07 and B-13. Further, the modified midpoint deflection over time  $u(t)$ , determined as

$$u(t) = u_{mid}(t) - u_{sup}(t) \quad (2)$$

is also presented. From this it can be noted that the magnitude and duration of the initial uplift at the support is about 3 mm and 5 ms (5 mm and 6 ms), respectively, for beam B-07 (B-13). Thereafter, the beam remains in contact with the support ( $u_{sup} \approx 0$  mm) until a duration of about 25 ms (40 ms), at which time the whole beam starts to lift due to its rebound. As comparison, the time of maximum deflection corresponds to about 12 ms (25 ms), which means that the beam is in contact with the support for a long enough time to regard the beam's boundary conditions as simply supported. For beam B-07, it can be seen that  $u(t)$ , during  $t \approx 25\text{--}60$  ms, oscillates around a deflection of about 18 mm, which corresponds to the permanent plastic deflection obtained in the beam due to impact loading, see Table 3.

In Leppänen et al. (2020), it was shown using nonlinear FE analyses, that the lack of support preventing uplift had negligible effect on both the  $u(t)$  response and the resulting crack pattern of impact loaded beams of similar geometry and load as that used in the tests presented here. Hence, it is judged that the influence of uplift did not have any major influence on the response of the tests carried out. However, the temporary uplift at the support caused the modified midpoint deflection  $u(t)$  to obtain a local leap in the curve, see Figure 6. This type of response was obtained for all the beams in the study subjected to impact loading.

In Figure 7, the modified midpoint deflection over time  $u(t)$  for the impact loaded beams are shown for all beams. The scatter of the results was generally small until the maximum deflection was reached but increased somewhat after that. Failure was not reached in any of the beams due to impact loading. It can be noted that the deflections obtained in the beams with prestretched bars were smaller than that obtained in beams with regular bars. This is an effect of beams with prestretched bars reaching a higher load capacity at a lower deflection, see more of this below in Section "Response at static loading", which means that for the impact loads used in these tests, the beams with prestretched reinforcement were more "effective" than beams with regular reinforcement. However, it does not mean that prestretched bars generally is a better solution than using regular bars.

From the impact loaded tests, it was not possible to predict how close a certain beam was to final failure. To investigate this, static tests were used to determine the residual capacity of the previously impact loaded beams, i.e., the residual capacity producing internal work that could balance the increased external work from a potentially more severe impact load.

### Response at static loading

The beams that were subjected to an impact load were subsequently statically loaded to evaluate their residual response, i.e., stiffness, load capacity and plastic internal work. For comparison,



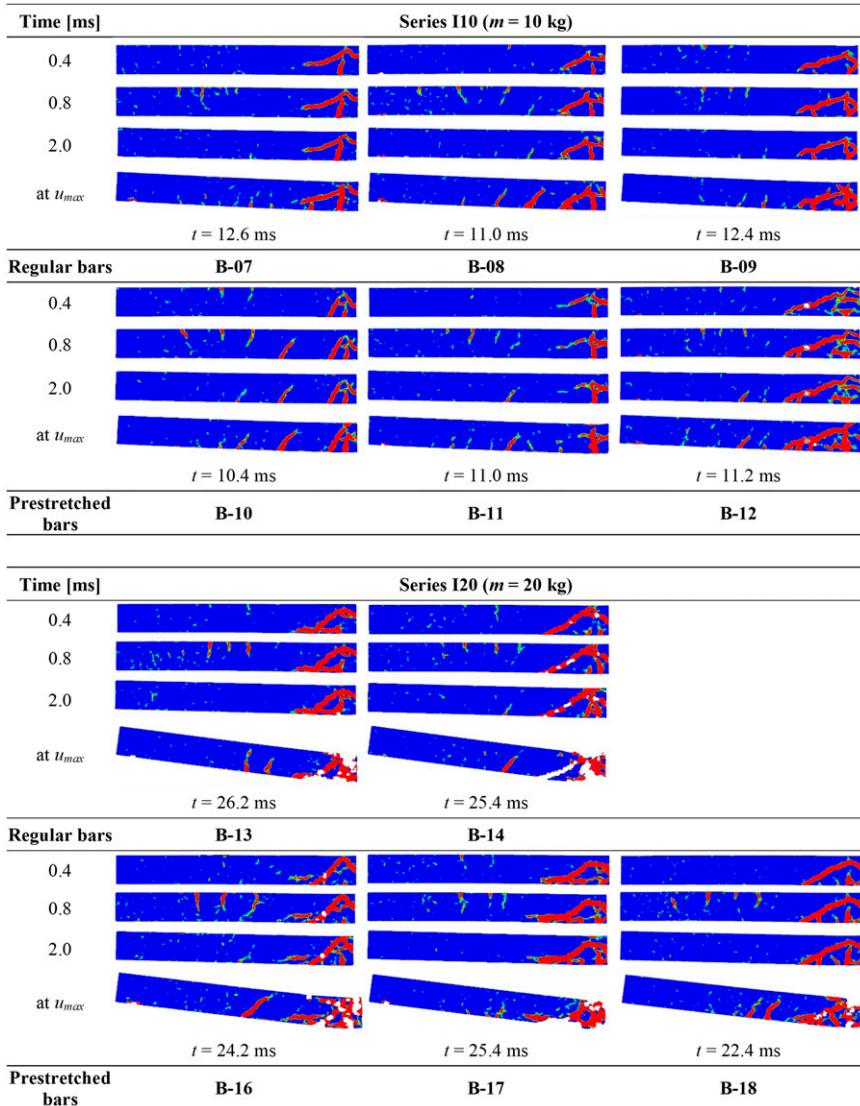


**Figure 5.** Initial crack pattern of all beams subjected to impact loading (red colour = crack, blue colour = uncracked concrete).

3 + 3 undamaged reference beams (i.e., beams that was not previously subjected to impact loading) were tested and the response, shown as load-deflection  $F(u)$  curves, of these tests are shown in Figure 8. The maximal load,  $F_{max}$ , was somewhat higher in the beams with prestretched bars than in the beams with regular bars, and this load was also obtained at less deflection of the beams. However, the maximum deflection at failure,  $u_{fail}$ , was considerably higher in the beams with regular bars than in beams with prestretched bars. Consequently, this indicates that the beams with prestretched bars produce a more effective resistance against less severe impact loads; that is, impacts that only cause a deflection  $u_{mid}$  of about 30 mm. For more

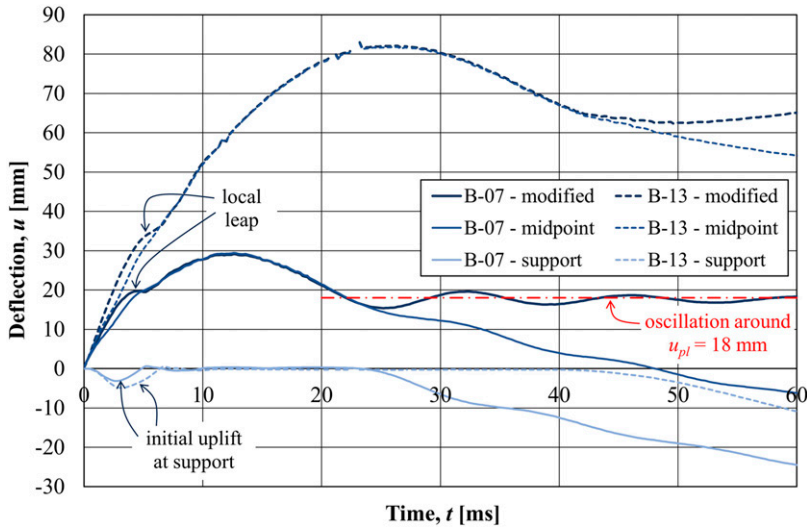


**Figure 6.** Deflection-time curves showing support uplift, midpoint deflection and modified midpoint deflection for beams B-07 and B-13 when subjected to impact loading.

severe impact loads, though, higher deflection will be obtained in the beam to withstand the load, and for such cases, the static response indicates that beams with regular bars would be more effective than beams with prestretched bars.

In Figure 9, the residual response  $F(u)$ , due to static loading, of the impact loaded beams in Series I10 are compared with the response of the corresponding reference beams in Series S. For the beams in Series I10, an initial plastic deflection already existed due to previous impact loading and in the graphs, this is indicated as an initial deflection at zero static load. The initial elastic stiffness of the impact loaded beams was very similar to that obtained in the cracked reference beams. When reaching a load level approximately corresponding to that of the load-deflection curves of the reference beams, reinforcement yielding occurred. This indicates that the initial residual response of the beams previously subjected to impact loading “tuned in” to the response of the statically loaded reference beams. This was true for all beams, regardless of type of bar used. In the beams with regular bars, though, the residual response showed an almost constant load plateau with substantially increased deflection at final failure (about 30–40 mm) compared to that obtained in the reference beams, see Figure 9(a). However, for the beams with prestretched bars, the residual response was more similar to that of the reference beams, even though the deflection at final failure increased (about 10–15 mm) here as well, see Figure 9(b). Final failure was in all these beams obtained due to reinforcement rupture. From Figure 9 it can be concluded that in these tests, previous impact loading had a positive effect on the residual response of the beams: the load capacity at a given deflection was similar or higher than in the reference beams, while the deflection  $u_{fail}$  increased significantly (some) for beams with regular bars (prestretched bars). This indicates that there is a beneficial effect to the beam’s structural response when subjected to impact loading compared to static loading.

In Figure 10, the residual response  $F(u)$ , due to static loading, of the impact loaded beams in Series I20 are shown. When subjected to impact loading, these beams obtained large plastic deformations, and because of this, considerable concrete damage also developed in the mid part of the

**Table 3.** Summary of results from impact and static tests.

Identification			Impact loading				Static loading			Total	
Series	Beam	Bars	$v_0$	$u_{max}$	$u_{pl}$	$W_{i,imp}$	$u_{fail}$	$F_{max}$	$W_{i,sta}$	$u_{fail,tot}$	$W_{i,tot}$
			[m/s]	[Mm]	[Mm]	[J]	[Mm]	[kN]	[J]	[Mm]	[J]
S	B-01	Regular	-	-	-	-	63.0	9.5	486	63.0	486
	B-02		-	-	-	-	54.4	9.7	432	54.4	432
	B-03		-	-	-	-	61.3	10.1	488	61.3	488
	<b>Average</b>	-	-	-	-	<b>59.6</b>	<b>9.8</b>	<b>469</b>	<b>59.6</b>	<b>469</b>	
S	B-04	Prestretched	-	-	-	-	32.1	9.7	254	32.1	254
	B-05		-	-	-	-	42.1	10.8	364	42.1	364
	B-06		-	-	-	-	38.6	10.1	311	38.6	311
	<b>Average</b>	-	-	-	-	<b>37.6</b>	<b>10.2</b>	<b>310</b>	<b>37.6</b>	<b>310</b>	
I10	B-07	Regular	9.83	29.1	18.0	239	87.0	7.7	391	105.0	630
	B-08		9.86	26.6	15.3	240	76.0	8.4	411	91.3	651
	B-09		9.83	27.9	17.5	239	77.3	8.0	406	94.8	645
	<b>Average</b>	<b>9.84</b>	<b>27.9</b>	<b>16.9</b>	<b>240</b>	<b>80.1</b>	<b>8.0</b>	<b>403</b>	<b>97.0</b>	<b>642</b>	
I10	B-10	Prestretched	9.84	24.5	12.0	239	36.3	8.9	186	48.3	425
	B-11		9.85	26.2	14.0	240	32.0	8.6	158	46.0	398
	B-12		9.82	25.2	12.1	238	41.8	8.6	235	53.9	473
	<b>Average</b>	<b>9.84</b>	<b>25.3</b>	<b>12.7</b>	<b>239</b>	<b>36.7</b>	<b>8.7</b>	<b>193</b>	<b>49.4</b>	<b>432</b>	
I20	B-13	Regular	9.80	82.1	69.1	652	27.6	8.1	99	96.7	751
	B-14		9.83	82.1	67.1	656	22.6	7.8	74	89.7	730
	B-15		-	-	-	-	-	-	-	-	-
	<b>Average</b>	<b>9.82</b>	<b>82.1</b>	<b>68.1</b>	<b>654</b>	<b>25.1</b>	<b>7.9</b>	<b>86</b>	<b>93.2</b>	<b>740</b>	
I20	B-16	Prestretched	9.90	74.7	58.6	662	25.3	8.7	88	83.9	750
	B-17		9.80	77.9	61.8	651	19.6	6.2	56	81.4	706
	B-18		9.82	70.0	55.5	650	24.3	9.5	80	79.8	730
<b>Average</b>	<b>9.84</b>	<b>74.2</b>	<b>58.6</b>	<b>654</b>	<b>23.1</b>	<b>8.1</b>	<b>74</b>	<b>81.7</b>	<b>729</b>		

$u_{max}$  = maximum deflection due to impact,  $u_{pl}$  = plastic deflection due to impact,  $W_{i,imp}$  = internal work of beam due to impact,  $u_{fail}$  = deflection at failure at static loading,  $F_{max}$  = maximum load at static loading,  $W_{i,sta}$  = internal work of beam at static loading (total internal work for Series S, plastic internal work for Series I10 and I20),  $u_{fail,tot} = u_{pl} + u_{fail}$  = total deflection due to impact and static loading,  $W_{i,tot} = W_{i,imp} + W_{i,sta}$  = total internal work from impact and static loading.

beam. This damage made it unsuitable to apply a point load in the middle of the beam, and instead four-point loading was used as shown in Figure 1(b). The different test set-ups used make a direct comparison with the reference beams difficult and here only a comparison of the residual response with regular and prestretched bars are made. In the beams with the regular bars, the residual response was very similar; both initial stiffness, maximum load, and total deflection at final failure. In the beams with prestretched bars, larger deviations in the response were obtained; however, the final failure was obtained at almost the same total deflection. Final failure was in beams B-16 and B-18 due to reinforcement rupture of at least one bar. However, in beams B-13, B14 and B-17, considerable load decrease was obtained due to a combination of large diagonal shear cracks and partial loss of the concrete compressive zone, resulting in a weak residual response at increased deflection, without reaching a distinct failure. The tests of these beams were instead stopped when the load capacity had decreased to about 2 kN.

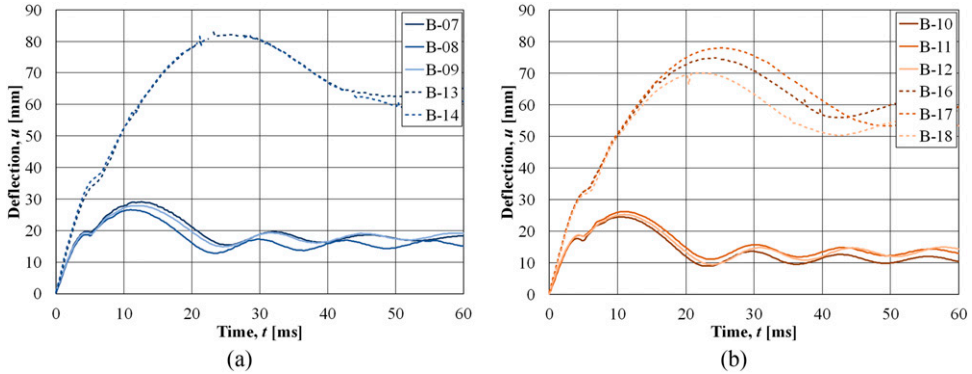


**Figure 7.** Modified midpoint deflection-time curves from impact tests of beams with (a) regular bars, and (b) prestretched bars.

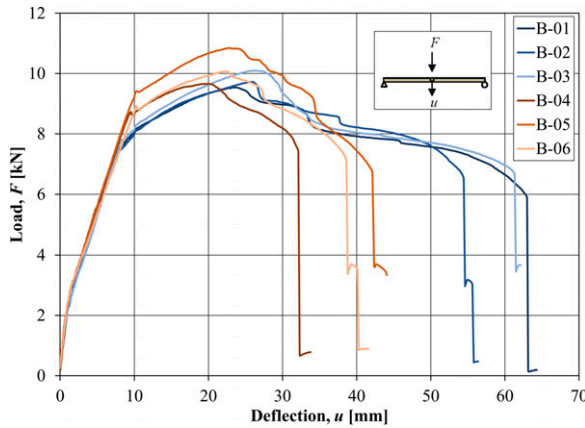


**Figure 8.** Load-deflection curves (static loading in three-point bending) for reference beams (regular bars: B-01 to B-03, prestretched bars: B-04 to B-06).

Crack patterns from all the static tests are shown in [Figure 11](#). For Series S and I10, the crack pattern shown are given at a deflection  $u_{mid} = 30$  mm (load level  $F_{30mm}$  listed in table) for the corresponding test. For Series I20, though, the crack pattern shown is given for a deflection when load  $F_{max}$  was obtained in the residual static tests (deflection  $u_{Fmax}$  listed in table). White regions in the crack pattern indicate loss of data due to spalling of the concrete cover, thus losing the speckle pattern on the concrete surface used in DIC.

For the statically loaded reference beams (Series S), typical vertical flexural cracks can be observed in [Figure 11](#). For the beams previously subjected to impact loading (Series I10 and I20), though, diagonal shear cracks are seen in the middle of the beam originating from the point of impact and the flexural cracks generally have a more skewed shape. This is because the crack patterns observed were originally created during the impact loading and during the following static loading the existing cracks re-opened again and continued to grow. Hence, for these beams, the

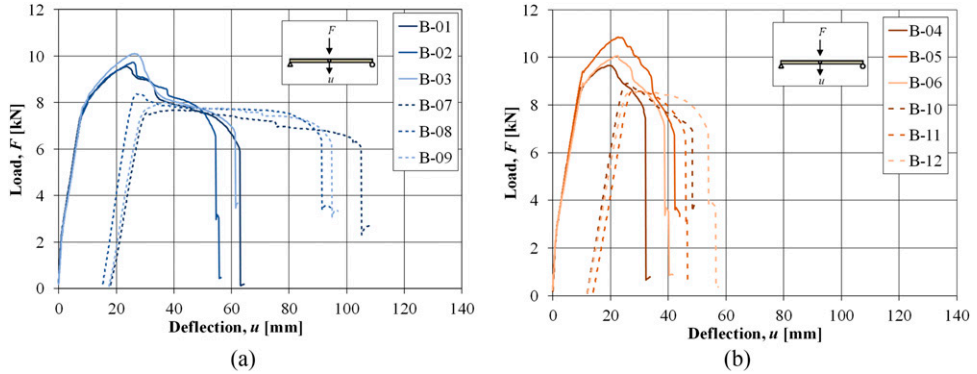


**Figure 9.** Comparison of load-deflection curves (static loading in three-point bending) for reference beams and beams first subjected to drop weight impact of mass 10 kg (Series I10): (a) regular bars, and (b) prestretched bars.

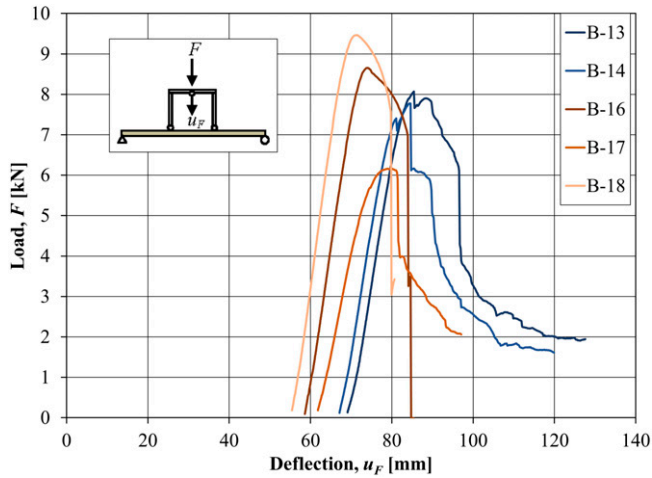


**Figure 10.** Load-deflection curves (static loading in four-point bending) for beams first subjected to drop weight impact of mass 20 kg (Series I20) (initial deflection when  $F = 0$  kN shows plastic deflection  $u_{mid}$  from impact loading).

crack pattern obtained by static loading is very similar to that obtained from the impact loading, compare with crack patterns at  $u_{max}$  in Figure 5.

### Summary of results

In Table 3, some key results from the impact and static tests are summarised. Apart from modified deflections  $u$  and maximum static load  $F_{max}$ , also the internal work  $W_i$  (i.e., the energy absorption) is listed in the table. In the static tests,  $W_{i,sta}^1$  was determined as the area under the  $F(u)$  curves in Figures 8 to 10. For Series S, this was done for the full  $F(u)$  curve up to a deflection  $u$  corresponding to when the post-peak load capacity had reached a load capacity  $F = F_{max}/2 \approx 5 \text{ kN}^2$ . Consequently,

Beam <i>F</i> 30mm	Series S	Beam <i>F</i> 30mm	Series I10 ( <i>m</i> = 10 kg)	Beam <i>uF</i> max	Series I20 ( <i>m</i> = 20 kg)
B-01 9.0 kN		B-07 7.5 kN		B-13 85.2 mm	
B-02 9.1 kN		B-08 8.2 kN		B-14 84.5 mm	
B-03 9.3 kN		B-09 7.7 kN		B-15	-
B-04 8.2 kN		B-10 8.6 kN		B-16 74.1 mm	
B-05 9.9 kN		B-11 8.6 kN		B-17 78.9 mm	
B-06 8.8 kN		B-12 8.5 kN		B-18 71.3 mm	

**Figure 11.** Crack patterns obtained in static tests (red colour = crack, blue colour = uncracked concrete).

the contribution to the internal work  $W_{i,sta}$  beyond this deflection was neglected. For Series I10 and I20, a similar concept was used for the static loading, but here the elastic part of the  $F(u)$  curve (i.e., up to the deflection at which reinforcement yielding was obtained) was not included in  $W_{i,sta}$ . This elastic contribution to the total internal work was not accounted for since it is already included in the internal work  $W_{i,imp}$  made when the beam was subjected to impact loading.

To estimate the internal work during impact loading, the same method as for static loading cannot be used. Instead, a simplified method based on energy equilibrium, theory of plastic impact and an equivalent single degree of freedom system (SDOF) as described in for example, [Johansson and Laine \(2012\)](#), was used to estimate the internal work  $W_{i,imp}$ .

The kinetic energy of the drop weight just prior to impact can be determined as

$$E_{k,0} = \frac{m_w \cdot v_0^2}{2} \tag{3}$$

where  $m_w = 10$  kg (20 kg) is the mass of the drop weight in Series I10 (I20) and  $v_0 \approx 9.9$  m/s is the expected impact velocity for a drop height of  $h = 5.0$  m. However, this energy does not correspond to the external work applied on the beam; for this, the influence of energy loss due to impact and change in potential energy also needs to be considered.

In [Figure 12](#), the velocities of the drop weight and beam midpoint (i.e., point of impact in beam) are shown for beams B-07 and B-13. From this, it can be seen that there are some variations in the velocities in the initial impact stage; for both tests there are at least three local impacts during the first 10 ms. However, the average velocities of drop weight and beam were similar in both tests until the beam rebounded, that is, after maximum deflection was obtained. This indicates that the assumption of plastic impact between drop weight and beam is reasonable. Therefore, plastic impact between the drop weight (mass  $m_w$ ) and beam (mass  $m_b$ ) was assumed and using conservation of momentum, the joint velocity  $v_{wb}$  of the mass and beam midpoint after impact can be expressed as

$$v_{wb} = \frac{m_w}{m_w + m_b} \cdot v_0 \tag{4}$$

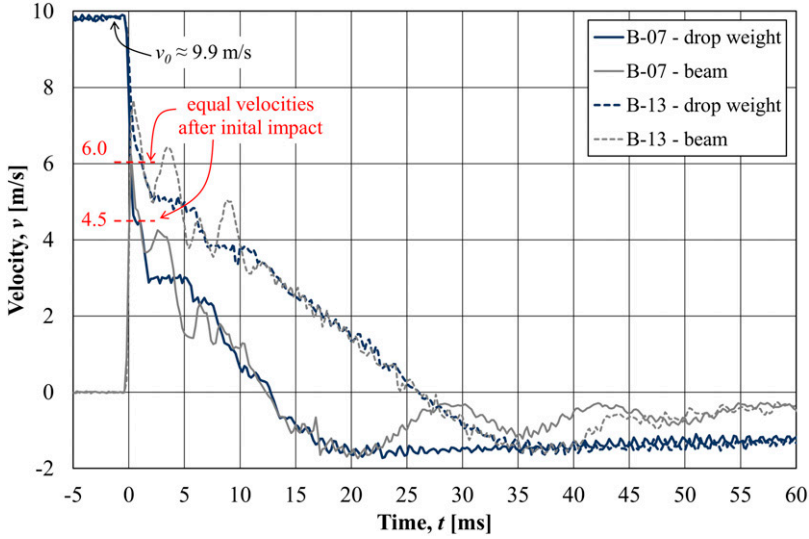


**Figure 12.** Velocities of drop weight and beam for beams B-07 and B13.

Here,  $m_b = \kappa_{LM} \cdot m_{beam}$  is the effective mass of the beam, in which  $\kappa_{LM}$  is a load-mass factor used to transform the beam to an equivalent SDOF system, see for example [Biggs \(1964\)](#). For the actual load case, a plastic response of the beam was obtained, giving  $\kappa_{LM} = 0.333$ , which together with  $m_{beam} = 32.5$  kg for the 1.3 m long beam part between the supports, gives  $m_b = 10.8$  kg. Using equation (4), the velocity after impact may be estimated as 4.8 m/s (6.4 m/s) for beams in Series I10 (I20). These estimates may also be compared with the velocities obtained after the first impact of beam B-07 (B-13) which were about 4.5 m/s (6.0 m/s), see [Figure 12](#). Hence, even though clearly not an ideal plastic impact, this assumption is still deemed to be sufficient for the purpose of estimating the internal work obtained in the beams due to impact loading.

$$E_{k,wb} = \frac{(m_w + m_b) \cdot v_{wb}^2}{2} \quad (5)$$

and combining this with equation (4), the external work acting on the beam due to impact may be estimated as

$$W_{e,k} = E_{k,wb} = \frac{m_w}{m_w + m_b} \cdot E_{k,0} \quad (6)$$

Further, additional external work  $W_{e,p}$ , caused by change in potential energy due to maximum beam deflection  $u_{max}$ , may be determined as

$$W_{e,p} = \left( m_w + \frac{m_{beam}}{2} \right) \cdot g \cdot u_{max} \quad (7)$$

in which  $g = 9.81$  m/s<sup>2</sup> is the gravitational acceleration. Finally, due to energy equilibrium, the external work applied to the beam is equal to the internal work done by the loaded beam and consequently, the internal work  $W_{i,imp}$  in a beam due to impact may be estimated as

$$W_{i,imp} = W_{e,k} + W_{e,p} \quad (8)$$



With input according to the above and using  $u_{max} \approx 0.03$  m (0.08 m) for Series I10 (I20), the internal work carried out by the beams due to impact loading can be estimated as  $W_{i,imp} \approx 243$  J (665 J) for Series I10 (I20). This estimate is approximate, and the influence of additional factors, for example wave propagation effects in the beam, not a fully plastic impact and influence of the beam's resistance, is neglected. For the tests presented here, this simplification is judged to provide small changes in the result and is therefore deemed to be acceptable. In Table 3, the presented values of  $W_{i,imp}$  differs somewhat from the values presented above due to small variations in the impact velocity  $v_0$  and value of  $u_{max}$  in the individual tests.

In Figure 13, the total internal work  $W_{i,tot}$  in Table 3 are compared. For Series S it can be concluded that the reinforcement ductility had high influence on  $W_{i,tot}$  when the beam was subjected to static loading only; here  $W_{i,tot}$  was in average a factor 1.51 higher when using regular bars compared to when using prestretched bars. This is also well in line with previous experience from static loading (CEB, 1998) and thus as expected. For beams in Series I10 it can be concluded that  $W_{i,tot}$  increased compared with that obtained in static loading only, but that the difference obtained due to reinforcement ductility remained similar to a factor 1.49.

However, for beams in Series I20, there was still an increase in  $W_{i,tot}$  compared to Series S and I10 but the difference in  $W_{i,tot}$  due to reinforcement ductility was negligible. That is, for these beams, in which the impact loading caused severe damage, there was insignificant difference of whether using regular bars or less ductile prestretched bars. Consequently, this response differs much to that observed in beams subjected to static load only. It also further indicates that the structural response obtained at impact loading may differ much compared to that of static loading. In all tests carried out here, though, the response obtained was improved due to impact loading; that is, the internal work increased with increased impact loading. In average,  $W_{i,tot}$  increased with a factor 1.37 (1.39) and 1.58 (2.35) in Series I10 and Series I20, respectively, in beams with regular (prestretched) bars. Consequently, it would have been conservative to use guidelines based on static loading for the estimation of internal work when designing the impact loaded beams studied here.

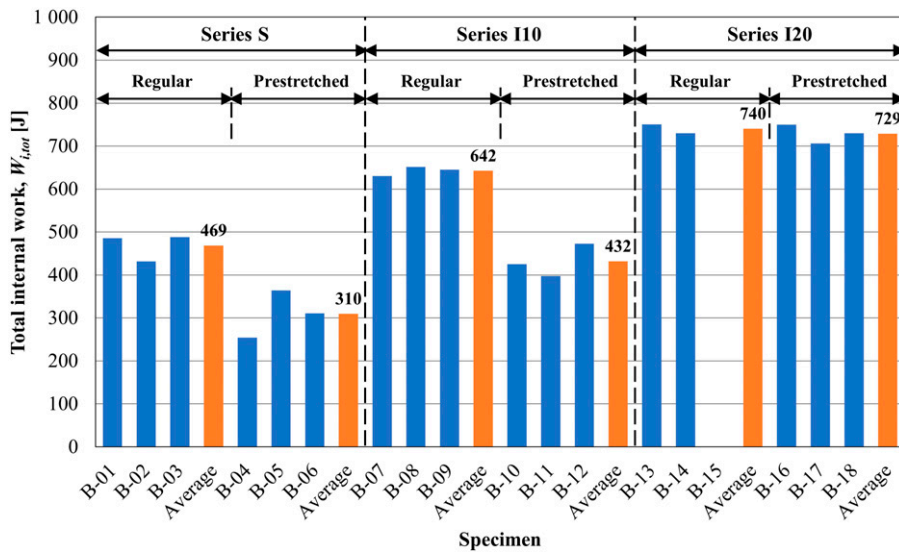


Figure 13. Comparison of total internal work.



It is believed that the increased plastic deflection, and hence the internal work, obtained in beams first subjected to impact loading, was mainly due to positive effects related to the appearance of diagonal shear cracks close to the impact zone. Thereby, the bond between reinforcement and concrete was weakened in this region, which meant that a larger part of the reinforcement could reach yielding prior to final failure. Consequently, the length of the plastic hinge increased, which resulted in larger plastic deflections and thus also increased internal work.

However, this hypothesis does not explain why there was negligible difference in  $W_{i,tot}$  for beams in Series I20 when using regular or prestretched bars. In beams with regular bars (beams B-13 and B-14), though, the load capacity at large deflection was limited by concrete crushing in the compressive zone, and hence the contribution to  $W_{i,sta}$ , due to still intact reinforcement, was small. Consequently, it is believed that if concrete crushing in these beams could have been further postponed (e.g., by using stronger concrete), regular bars would also have resulted in an increased amount of total internal work  $W_{i,tot}$ .

## Conclusions

The aim of this study was to examine the effect of various ductility of reinforcement bars used in concrete beams subjected to impact loading. Impact tests, using a steel drop weight with mass 10 kg or 20 kg and a drop height of 5.0 m, were carried out. To examine the residual response after impact loading, the beams were subjected to static loading until failure and from this, the total internal work in the beams was determined.

The following conclusions can be drawn:

- In all cases, previous impact loading had a positive effect on the residual response of the beams studied; that is, the internal work of the beams increased with increased impact loading.
- For pure static loading, and combination of mild impact loading (mass 10 kg) and static loading, the total internal work was about 50 % higher in beams with regular bars compared to beams with less ductile prestretched bars.
- For beams first subjected to severe impact loading (mass 20 kg), the total internal work increased further but the effect of various reinforcement ductility was negligible. However, it is believed that if concrete crushing in the compressive zone could have been further postponed, for example, by increasing the concrete strength, the beams with regular bars would have resulted in higher increased total internal work than the beams with prestretched bars.
- The response observed for beams subjected to severe impact loading differs from that obtained in static loading and is a further proof that the structural response obtained at impact loading may differ much compared to that obtained at static loading. Still, it can be concluded that it would have been conservative to use guidelines based on static loading for the estimation of internal work when designing the impact loaded beams studied here.
- High-speed camera in combination with Digital Image Correlation (DIC) analysis has proved to be a powerful tool for studying the structural response of impact loaded concrete beams where it can be used to study for example, crack propagation and deformations. An additional advantage with DIC is that the parameters that are of interest do not need to be known or specified beforehand, that is, if images of acceptable resolution are available it is possible to determine what type of results are of interest at a later stage. Compared to conventional measuring techniques, this is a considerable advantage.

## Acknowledgements

This research has been carried out at Chalmers University of Technology and the authors would like to thank the financier's representative Lars Gråbergs (BSc), from the Swedish Civil Contingencies Agency (MSB). Thanks also to research engineer Sebastian Almfeldt (M.Sc.), Chalmers, responsible for carrying out the experiments, and Mathias Flansbjer (PhD), Rise, responsible for the high-speed camera and help with DIC. Additionally, Leo Laine (PhD), member of the West Coast Sweden Shock Wave Group, is highly acknowledged for his support.

## Declaration of conflicting interests

The author(s) declared no potential conflicts of interest with respect to the research, authorship, and/or publication of this article.

## Funding

The author(s) disclosed receipt of the following financial support for the research, authorship, and/or publication of this article: This work was supported by the Swedish Civil Contingencies Agency (MSB). Additional funding for the experiments was provided by Fortifikationskårens forskningsfond (Fortification corps' research fund).

## ORCID iD

Morgan Johansson  <https://orcid.org/0000-0003-0020-0646>

## Notes

1. Results from three-point bending tests (Series S, Series I19) and four-point bending tests (Serie I20) cannot be directly compared with each other; however, here an approximate comparison is made using the following concept. It is possible to show that for the same simply supported beam, the forces  $F_{3p}$  and  $F_{4p}$  at three-point and four-point bending, respectively, causes the same maximal span moment  $M_{mid}$  if  $F_{3p} = F_{4p}/\alpha$ . Further, if at four-point bending a plastic hinge is obtained in the middle of the beam, the relation between the plastic deflection  $u_{4p,mid}$  in this position and deflection  $u_{4p,F}$  under the applied load can be expressed as  $u_{4p,mid} \approx \alpha \cdot u_{4p,F}$ . Hence, this means that the plastic internal work  $W_{i,pl}$ , that is, the area under  $F(u)$  at plastic response, would be approximately the same in three-point and four-point bending when comparing  $F_{3p}(u_{3p,mid})$  and  $F_{4p}(u_{4p,F})$ . Finally, for the test set-ups shown in [Figure 1](#), the factor  $\alpha = 0.65/0.50 = 1.3$ .
2. All beams were interrupted prior to reaching complete failure (i.e.,  $F = 0$  kN) and using this concept meant that the result could be directly compared with each other. For the beams included in this study, failure was in all cases reached due to the rupture of one or two reinforcement bars, hence resulting in a sudden drop of load capacity. Consequently, using this method, the internal work not accounted for in  $W_{i,sta}$  was negligible.

## References

- Adhikary SD, Li B and Fujikake K (2015) Residual Resistance of impact damaged reinforced concrete beams. *Magazine of Concrete Research* 67(7): 364–378.
- Andersson M and Pettersson E (2019) Reinforced concrete beams subjected to drop-weight impact. In: *Department of Architecture and Civil Engineering*. Gothenburg, Sweden: Chalmers University of Technology. Master's Thesis ACEX30-19-27.
- Biggs JM (1964) *Introduction to Structural Dynamics*. New-York, USA: McGraw-Hill.

- Bischoff PH and Perry PH (1991) Compressive behaviour of concrete at high strain rates. *Materials and Structures* 24: 425–450.
- CEB (1998) Ductility of reinforced concrete structures. Lausanne, Switzerland: CEB, Vol. 242.
- Cotsovos DM, Stathopoulos ND and Zeris CA (2008) Behavior of RC beams subjected to high rates of concentrated loading. *Journal of Structural Engineering* 134(12): 1839–1851.
- DOD (2008) *Structures to Resist the Effects of Accidental Explosions*. USA: Department of Defense. UFC 3-340-02.
- Fortifikationsverket (2011) *Fortifikationsverkets konstruktionsregler FKR 2011 (Swedish fortifications agency building regulations FKR 2011 Swedish)*. Sweden: Fortifikationsverket.
- Fujikake K, Senga T, Ueda N, et al. (2006) Study on impact response of reactive powder concrete beam and its analytical model. *Journal of Advanced Concrete Technology* 4(1): 99–108.
- Fujikake K, Li B and Soeun S (2009) Impact response of reinforced concrete beam and its analytical evaluation. *Journal of Structural Engineering* 135(8): 938–950.
- GOM Correlate (n. d). GOM Correlate Professional, Hotfix 5. <https://www.zeiss.com/metrology/en/software/metrology-software.html>
- Isaac P, Darby A, Ibell T, et al. (2017) Experimental investigation into the force propagation velocity due to hard impacts on reinforced concrete members. *International Journal of Impact Engineering* 100: 131–138.
- Johansson M and Laine L (2012) *Bybyggelsens motståndsförmåga mot extrem dynamisk belastning, Del 3: Kapacitet hos byggnader (Housing settlement capacity against extreme dynamic loading, Part 3: building capacity Swedish)*. Karlstad, Sweden: Publication MSB142, Swedish Civil Contingencies Agency.
- Johansson M and Rempling R (2016) Design of impulse loaded concrete structures: a comparison of FKR 2011 with various design regulations. In: *Report 2016-16, Department of Architecture and Civil Engineering*. Gothenburg, Sweden: Chalmers University of Technology.
- Leppänen J (2024) Dataset of article: residual capacity of RC beams subjected to impact loading: influence of reinforcement ductility. DOI: [10.5281/zenodo.11181111](https://doi.org/10.5281/zenodo.11181111)
- Leppänen J, Johansson M and Grassl P (2020) On the dynamic response of reinforced concrete beams subjected to drop weight impact. *Finite Elements in Analysis and Design* 180: 103438.
- Magnusson J, Hallgren M and Ansell A (2014) Shear in concrete structures subjected to dynamic loads. *Structural Concrete* 15(1): 55–65.
- Malvar LJ and Ross CA (1998) Review of strain rate effects for concrete in tension. *ACI Materials Journal* 95(6): 735–739.
- Peterson V and Ansell A (2022) Static and dynamic four-point flexural tests of concrete beams with variation in concrete quality, reinforcement properties and impact velocity. *Nordic Concrete Research* 65(2): 19–38.
- Pham TM and Hao H (2017) Plastic hinges and inertia forces in RC beams under impact loads. *International Journal of Impact Engineering* 103: 1–11.
- Saatci S and Vecchio F (2009) Effects of shear mechanisms on impact behavior of reinforced concrete beams. *ACI Structural Journal* 106(1): 78–86.
- Sutton MA, Ortu JJ and Schreir H (2009) *Image Correlation for Shape, Motion and Deformation Measurements*. New York, USA: Springer US.
- Ulzurrún GSD and Zanuy C (2017) Enhancement of impact performance of reinforced concrete beams without stirrups by adding steel fibers. *Construction and Building Materials* 145: 166–182.